JACS
JOURNAL OF THE AMERICAN CHEMICAL SOCIETY
Article
pubs.acs.org/JACS

Structure and Mobility of Metal Clusters in MOFs: Au, Pd, and AuPd Clusters in MOF-74

Lasse B. Vilhelmsen,[†] Krista S. Walton,[‡] and David S. Sholl*[,‡]

[†]Interdisciplinary Nanoscience Center (iNANO) and Department of Physics and Astronomy, Aarhus University, DK-8000 Aarhus C, Denmark

[‡]School of Chemical and Biomolecular Engineering, Georgia Institute of Technology, Atlanta, Georgia 30332-0100, United States

Supporting Information

ABSTRACT: Understanding the adsorption and mobility of metal−organic framework (MOF)-supported metal nanoclusters is critical to the development of these catalytic materials. We present the first theoretical investigation of Au-, Pd-, and AuPd-supported clusters in a MOF, namely MOF-74. We combine density functional theory (DFT) calculations with a genetic algorithm (GA) to reliably predict the structure of the adsorbed clusters. This approach allows comparison of hundreds of adsorbed configurations for each cluster. From the investigation of Au_8, Pd_8, and Au_4Pd_4 we find that the organic part of the MOF is just as important for nanocluster adsorption as open Zn or Mg metal sites. Using the large number of clusters generated by the GA, we developed a systematic method for predicting the mobility of adsorbed clusters. Through the investigation of diffusion paths a relationship between the cluster's adsorption energy and diffusion barrier is established, confirming that Au clusters are highly mobile in the MOF-74 framework and Pd clusters are less mobile.

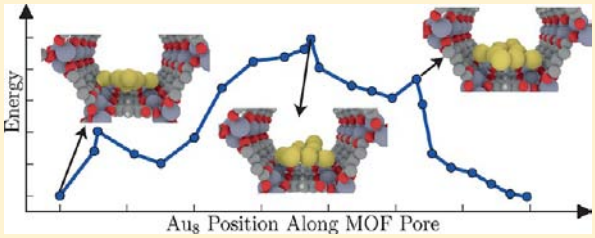

INTRODUCTION

Metal−organic frameworks (MOFs) are a class of nanoporous materials synthesized by mixing metals with organic ligands to produce a periodic framework.[1,2] MOFs can be made with different pore and cavity diameters, and a large number of one-dimensional (1D), 2D, and 3D connected MOFs have been reported.[3] The chemical environment of a MOF can be tuned by exposing the open metal sites, changing the MOF building blocks, or by functionalization. The diversity with which these parts can be combined makes it possible to generate thousands of different MOFs.[4−6] MOFs show promising applications in gas-separation[7,8] and storage,[9,10] drug delivery,[11] sensing,[12] and catalysis.[13−15] In the context of catalysis, MOFs have been shown to be capable of stabilizing nanosized metal clusters with a cluster size comparable to the pore diameter of the MOF.[16−18] These pore diameters are typically less than 2 nm, which is an ideal size for catalytically active particles.[19] This observation, combined with the possible interplay between the framework and the metal cluster in a catalytic reaction makes MOF-supported metal clusters interesting as possible catalysts.

The first report on metal loading in MOFs was made by Fischer et al. in 2005 for Pd in MOF-5.[20] Later investigations have focused on either MIL-101,[16,21−23] ZIF-8,[17,24−26] or MOF-5[18,20,27] using Au, Ag, Pd, and Ru deposition. Jiang et al. have shown how Au supported in ZIF-8 can catalyze the CO-oxidation reaction.[17] Gu et al. showed that Au−Pd clusters adsorbed in activated MIL-101 effectively catalyze the dehydrogenation of formic acid.[16] Recently Lu et al. reported how an array of different metal particles can be distributed homogenously in ZIF-8 by coating the metal clusters prior to synthesizing the MOF around the clusters.[26] Since this technique builds the MOF around the clusters, it improves the likelihood of the clusters being inside the framework instead of on the surface of the MOF, which is a significant concern.[21,28]

Although theoretical calculations have answered many questions associated with MOFs,[29,30] to our knowledge no theoretical investigations have been made for the adsorption of metal clusters in MOFs. One reason is the complicated surface structure of MOFs, making it difficult to convincingly predict the most stable geometries of adsorbed metal clusters. If this challenge can be overcome, calculations could be valuable in predicting and understanding which local environments in the MOF stabilize the metal particles the most. It is, for instance, an open question whether or not open metal sites, like those in MIL-101 and Cu-BTC, play a crucial role in metal particle adsorption as they do in CO_2 and H_2 adsorption.[31,32]

While there are no previous theoretical studies of metal clusters in MOFs, a large literature exists associated with theoretical descriptions of small metal clusters on two-dimensional surfaces.[33,34] In this paper, we adapt some recent, efficient methods from previous work on flat surfaces[35] to predict the structure and mobility of small metal clusters in a MOF. In particular, we show how density functional theory (DFT) calculations combined with a genetic algorithm (GA) can be used to predict the structure of MOF-supported metal clusters. The investigation will focus on the adsorption of Au

Received: May 23, 2012
Published: June 27, 2012

   dx.doi.org/10.1021/ja305004a | J. Am. Chem. Soc. 2012, 134, 12807−12816

and Pd. Au is chosen because of its interesting applications in catalysis and the challenges associated with immobilizing Au.[19] Pd is chosen because it is expected to have a stronger interaction with the MOF and because synergistic effects exist between Au and Pd for reactions such as the acetoxylation of ethylene[36] and dehydrogenation of formic acid.[37] The Au and Pd clusters will be adsorbed in MOF-74.[38] MOF-74, with the formula Zn_2(2,5-dihydroxyterephthalate), consists of infinite helical rods of Zn connected by DHBDC linkers forming a 1D connected network. The structure within a given rod alternates between a chain of Zn/O atoms and a benzene ring (see Figure 1). The Zn atoms are open metal sites since they only

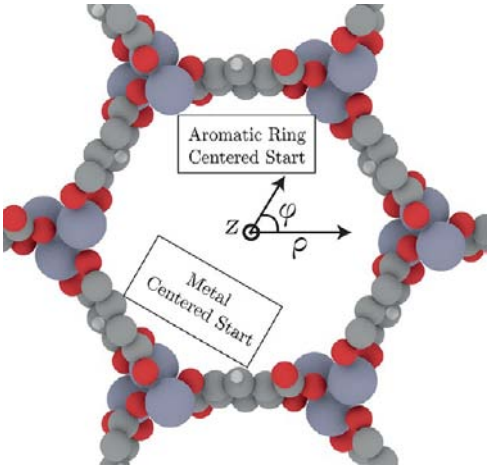

Figure 1. Side view of MOF-74. A cylindrical coordinate system is used to describe positions within the MOF. The MOF has a six-fold rotational symmetry. The boxes used to generate random starting populations for the GA runs are shown. Atoms are shown in red (oxygen), gray (carbon), white (hydrogen), and light purple (zinc).

coordinate to five oxygen atoms. MOF-74 is thus a good MOF for probing the importance of open metal sites for metal cluster adsorption. Variants of MOF-74 can be synthesized with Zn substituted with Mg, Mn, Co, or Ni,[31] which will be exploited in this contribution to investigate both the Zn and Mg variants.

To provide fundamental insight into metal cluster adsorption in MOFs, we present a systematic investigation of the adsorption of Au_1 and Pd_1, followed by the adsorption of Au_8, Pd_8, and Au_4Pd_4 as found with the GA. Although it is not readily possible with DFT calculations to investigate significantly larger clusters, we show that from these clusters it is possible to gain insight into the importance of the open metal sites and the stability of the different metals in the MOF. Our calculations assume that the clusters are directly coordinated with the MOF, not covered in any kind of capping ligand. Although most experiments with metal clusters in MOFs to date have used routes that generate ligand-capped clusters, bare clusters have been extensively examined in experiments with solid substrates.

There is no topological feature of MOF-74 that limits the growth of metal particles within each rod of the framework. In thermodynamic equilibrium it is thus expected that all metal loaded into each rod of the MOF will agglomerate together. However, from the large number of structures found for Au_8 and Pd_8, upper bounds can be calculated for the diffusion barrier for motion of the metal clusters along the framework pore. These results provide information regarding the time scale over which agglomeration into larger particles will happen. It is important to investigate the diffusion of these particles in the MOF, since arguably the biggest challenge in Au catalysis is the difficulties associated with stabilizing isolated Au clusters with a diameter less than a few nanometers.[19]

■ COMPUTATIONAL METHODS

To study metal cluster adsorption in a MOF a computational method is needed which describes both the formation of covalent bonds and includes the flexibility of the framework. The standard method for such investigations is a DFT-based approach. The present study uses the grid-based projector augmented wave (GPAW) DFT code[39,40] which is based on the PAW formalism by Blöchl[41] with a real-space grid based (GB) basis. Besides the GB basis, GPAW also offers a linear combination of atomic orbitals (LCAO) basis. For the systems we studied, a total energy calculation with the LCAO basis is approximately 6 times faster than with the GB basis. We therefore used the LCAO basis to do fast initial relaxations and then the GB basis for a more precise relaxation for each structure considered.[42] For the LCAO calculations a dzp-basis was used, and a grid spacing of 0.19 Å is used for all calculations in both modes. Except when otherwise stated, the calculations are without spin.

The accuracy of a DFT calculation is largely determined by the choice of exchange-correlation functional. We used the standard Perdew−Burke−Ernzerhof (PBE) generalized-gradient approximation (GGA) functional.[43] The PBE functional successfully describes covalently bonded systems although its description of Au[35,44] tends to underestimate the interaction between small Au clusters and substrates.[35] To gauge the reliability of the PBE functional the meta-GGA M06-L[45] was used for a limited number of calculations. M06-L is a fitted functional that includes the kinetic energy density besides the quantities used by GGAs. The M06-L functional has been shown to improve the description of molecular systems[45] while also improving the description of Au clusters[44] and benzene adsorption.[46] It has been termed "dispersive aware"[47] and for some systems outperforms the widely used hybrid B3LYP.[48] The M06-L functional is however computationally more expensive than the PBE functional and has inherent numerical instabilities, making an investigation with only this functional too costly.

The experimental crystal structure of MOF-74 was obtained from ref 38, and a 2 × 1 × 1 replication of the primitive cell was used for all adsorption studies. A side view of the structure is shown in Figure 1. All calculations were performed with lattice parameters obtained from DFT optimization of the MOF. The volume of the optimized unit cell expands by 5.5% compared to the experimental structure. The DFT optimized primitive unit cell is (a, b, c) = (6.96 Å, 15.42 Å, 15.42 Å), (α, β, γ) = (117.78°, 98.65°, 98.65°). The angles and the ratio between a and b are, within experimental uncertainties, unchanged compared to the experimental ones. For optimizing the unit cell a k-point spacing of 2 × 1 × 1 was used, while gamma-point calculations are sufficient for all adsorption studies in the 2 × 1 × 1 supercell. The typical spacing between the studied clusters in the 2 × 1 × 1 supercell is 7−8 Å.

A severe challenge in understanding the structure of nanoclusters of atoms is the very large number of possible atomic configurations that can be formed.[34,49−51] It is computationally feasible to systematically explore the configurations available to clusters containing 1−3 atoms "by hand", but for a reliable treatment of larger clusters, methods that automatically generate a diverse range of candidate structures are required. All adsorbed cluster geometries were found with a recently implemented genetic algorithm (GA) developed for adsorbed clusters.[35] The GA follows the scheme proposed by Deaven and Ho[49] with several improvements making the method more suitable for use with computationally expensive DFT calculations.[35]

A GA consists of several steps. First a random starting population is generated. For cluster adsorption on surfaces which have a small unit cell compared to the cluster, this starting population typically spans several unit cells.[35] For adsorption in a MOF, where the unit cell is comparable or larger than the cluster, care needs to be taken in how the starting population is distributed. MOF-74 has a cylindrical pore, so the cylindrical coordinate system shown in Figure 1 is used to

dx.doi.org/10.1021/ja305004a | J. Am. Chem. Soc. 2012, 134, 12807−12816

describe positions in the MOF. We ensured that clusters were tested throughout the unit cell by characterizing each cluster by its center-of-mass and verifying the presence of clusters throughout the cell. To ensure that clusters are tested for all combinations of (z, ϕ), two separate runs of the GA are made for each stoichiometry. One run is made with the starting population centered on $\phi = 0°$, while the other is centered on $\phi = 30°$. To ensure a uniform distribution in the z direction, the starting population is varied such that its center of mass varies from $z = 0$ Å to $z = 6.96$ Å, corresponding to one unit along the z axis. Each starting candidate is generated by randomly distributing the atoms within a box as shown in Figure 1. The length of the box in the z direction is equal to one unit cell height (6.96 Å). A candidate is discarded if an atom is unreasonably close to another atom either in the cluster or the framework. For each run a starting population of 40 candidates is used and each run of the GA includes between 139 and 255 tested candidates.

The starting population is treated as all other proposed candidates generated by the GA. The candidates are first relaxed in LCAO mode and subsequently with the GB basis until the maximum force on any atom is below 0.05 eV/Å. A population of the 15 lowest energy and structurally different candidates is maintained and used to propose new structures. Both energy and internal structure are used to determine if two GA structures are equivalent. For two structures to be considered equivalent, the energy difference between the two structures needs to be smaller than $\Delta E = 0.02$ eV, while the relative signed difference between a sorted list of all interatomic distances for each cluster needs to be smaller than $d_{rel} = 1.5\%$ with no single difference larger than $d_{max} = 0.7$ Å.[35]

To ensure a survival of the fittest scheme the most stable candidates need to be selected for pairing more frequently than their less stable counterparts. In ref 52 it is proposed to assign a fitness (F_i) to each candidate in the population and select candidates with a probability (P_i) proportional to this fitness. To help ensure a diverse population we chose to multiply P_i with a uniqueness factor U_i that decreases the probability of candidate i if it has previously been used for pairings or structures existing similar to it outside of the population. F_i and U_i are defined as

$$F_i = \frac{1}{2}[1 - \tanh(2\rho_i - 1)], \quad \rho_i = \frac{E_i - E_{min}}{E_{max} - E_{min}},$$

$$U_i = \frac{1}{\sqrt{1 + n_i}} \cdot \frac{1}{\sqrt{1 + m_i}}$$

where $P_i = F_i \cdot U_i$. E_{min} (E_{max}) is the minimum (maximum) energy of any structure in the population, n_i is the number of times candidate i has participated in a pairing, and m_i is the number of candidates which are structurally similar to the ith candidate but not included in the population. The functional form of U_i is constructed such that unique new structures do not have their fitness reduced and old candidates are not penalized too heavily. The inclusion of U_i is a new addition to GA optimization methods.

When two structures have been selected for pairing, they are paired together using the cut-and-splice operator proposed by Deaven and Ho.[49] After pairing there is a 50% probability that the candidate undergoes one of two mutations: (1) rattling of 40% of the atoms in a random direction with random amplitude up to 1.6 Å or (2) one pair of atoms with different atomic numbers is permutated. Both mutations have been reported elsewhere.[52] For more details on the GA we refer the reader to the Supporting Information of ref 35.

For the analysis of the adsorbed atoms and clusters it is helpful to look at the charge arrangement in the MOF. We employ the density derived electrostatic and chemical (DDEC)[53,54] net atomic charges method for this. The DDEC method has been shown to reproduce chemically meaningful charges for a large set of both condensed and porous materials, and it is therefore suitable for this investigation.

RESULTS AND DISCUSSION

Adsorption of Au_1 and Pd_1 in MOF-74. Before studying the adsorption of clusters it is instructive to study the adsorption of single metal atoms to gauge the different adsorption sites in the framework. To systematically test the adsorption of Au_1 and Pd_1 a grid of 25 candidate positions was distributed across the unique part of the unit cell. Five unique z values were chosen (corresponding to 1.39 Å between each candidate), and five values of ϕ were chosen to span the 60° interval. The radial coordinate was adjusted to follow the shape of the MOF pore. Using these estimates as starting positions, Au and Pd were relaxed separately. Both the metal atoms and the atoms making up the MOF framework were allowed to relax in these calculations. The four most stable configurations are shown in Figures 2 and 3 for Au and Pd, respectively. For

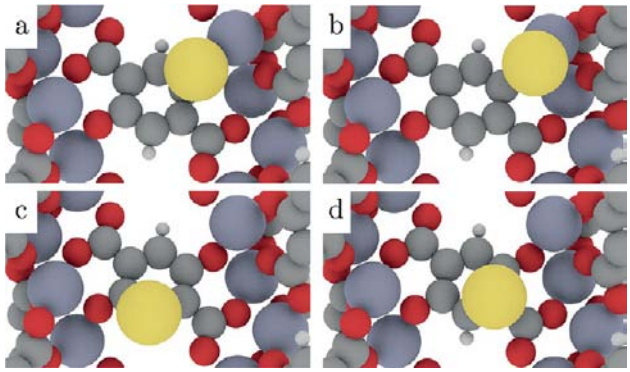

Figure 2. The four most stable Au_1 adsorption configurations. The yellow atom is Au. Bond distances are shown in Table 1.

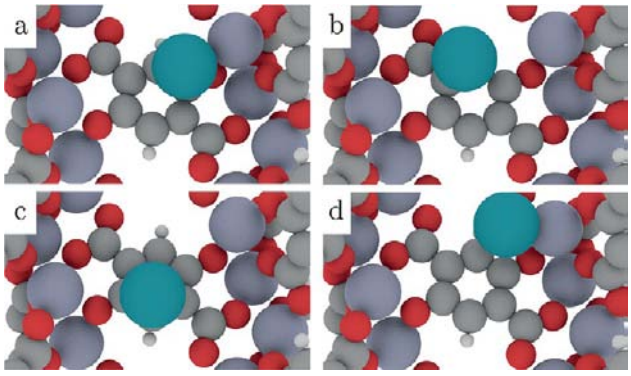

Figure 3. The four most stable Pd_1 adsorption configurations. Palladium is colored dark blue. Bond distances are shown in Table 1.

Au the calculations were done with spin polarization with an initial magnetic moment on the Au atom since Au has one unpaired 6s electron. Adsorption energies and local coordina-

Table 1. Adsorption Potential Energies, Local Coordination, and DDEC Charge of the Adsorbed Metal Atoms Seen in Figures 2 and 3

structure	E_b (eV)	bond lengths (Å)	DDEC charge (e)
Au_1 (Figure 3a)	−0.66	Zn: 2.6, C: 2.5	−0.24
Au_1 (Figure 3b)	−0.61	Zn: 2.5	−0.29
Au_1 (Figure 3c)	−0.45	C: 2.2	−0.13
Au_1 (Figure 3d)	−0.24	C: 2.4	−0.16
Pd_1 (Figure 4a)	−1.44	C: 2.1, 2.2, Zn: 2.8	0.16
Pd_1 (Figure 4b)	−1.38	C: 2.1, 2.2	0.18
Pd_1 (Figure 4c)	−1.21	C: 2.1	0.14
Pd_1 (Figure 4d)	−0.88	Zn: 2.5, O: 2.2	0.13

dx.doi.org/10.1021/ja305004a | J. Am. Chem. Soc. 2012, 134, 12807−12816

tion are reported in Table 1. The adsorption energies are defined as

$$E_b = E_{tot} - (E_{MOF} + E_{metal}) \quad (1)$$

with E_{tot} being the energy of the MOF including the adsorbed atom, E_{MOF} the energy of the relaxed MOF-74 framework without any adsorbed species, and E_{metal} the energy of the metal atom alone in the same super cell as the MOF. Bond lengths are reported for all atoms within a distance of 15% of the shortest distance observed for two such atoms.

It is clear from Table 1 that Pd is bound more strongly to the MOF than Au. This is unsurprising since Pd is generally more reactive than Au. What is surprising is that the open metal site, which plays a crucial role in H_2[31] and CO_2[32] adsorption in MOF-74 and Mg-MOF-74, respectively, does not offer significantly stronger binding sites than the aromatic ring. The best adsorption site for both Au and Pd involves the joint attachment of the metal atom to both Zn and C atoms in the framework. For Au the second best adsorption site is coordinated only to a Zn atom, with the Au−Zn bond pointing away from the framework. The loss of bonds to the aromatic ring decreases the binding by 0.05 eV relative to the most stable site, whereas a binding site only involving the ring system reduces the binding energy by 0.21 eV. For Pd the three most stable adsorption sites all involve carbon, but only one of them involves Zn. In this case the decrease in bond strength going to a Zn-free adsorption site is only 0.06 eV, compared to the most stable site not involving the aromatic ring having a binding energy that is 0.56 eV weaker.

The DDEC charges in Table 1 show that Au adsorbed on the Zn site gains more charge from the framework than when adsorbed on sites not involving Zn. This charge transfer is not surprising since the electronegativity of Au is significantly higher than that of Zn. The charge gained by the Au atom is not, however, transferred directly from the Zn atom. For the two most stable Au adsorption sites the charge difference on the Zn atoms before and after Au adsorption is $-0.23e$ and $-0.22e$. The Zn atoms thus also gain charge during Au adsorption, with the charge mostly being transferred from neighboring O atoms which lose $0.34e$ and $0.37e$ in the two cases. The remaining charge is donated from the C atoms. For Au the weak binding can thus be understood as an unfavorable charge rearrangement in the framework. For Pd the charge rearrangement in the framework can be described more simply. For the three most stable adsorption sites the charge lost by the Pd atom is donated directly to the C atoms in the vicinity of the adsorption site. For all four adsorption sites the charge difference on the C atoms are within $0.02e$ of the charge lost by the Pd atom. The binding is thus a clear covalent bond with charge redistribution between the Pd atom and the nearby carbon atoms.

Adsorption of Au_8, Pd_8, and Au_4Pd_4 in MOF-74. Having established that all parts of the MOF can bind both Au and Pd with no clear preference for any part of the MOF, we now move on to the more complex investigation of cluster adsorption in the framework. The first part of this section will focus on the identification of the relevant Au_8, Pd_8, and Au_4Pd_4 structures with the later part analyzing the observed structures.

The interior surface of MOF-74 exposes Zn, C, O, and H atoms organized in a nonsymmetric way within each unit cell. An approach to convincingly predict the structure of an extended cluster in this framework must necessarily involve some kind of systematic method. GAs have shown success in this area[35,55] and we chose, as already described in the computational section, to use such a method. Two separate runs of the GA are performed for each stoichiometry, one centered on the Zn chain (referred to as metal in the figures) and one on the aromatic ring (referred to as ring in the figures). As an example of this approach, the adsorption energies of all of the Au_8 clusters examined are shown as a function of their center of mass coordinates in Figure 4. This data set includes

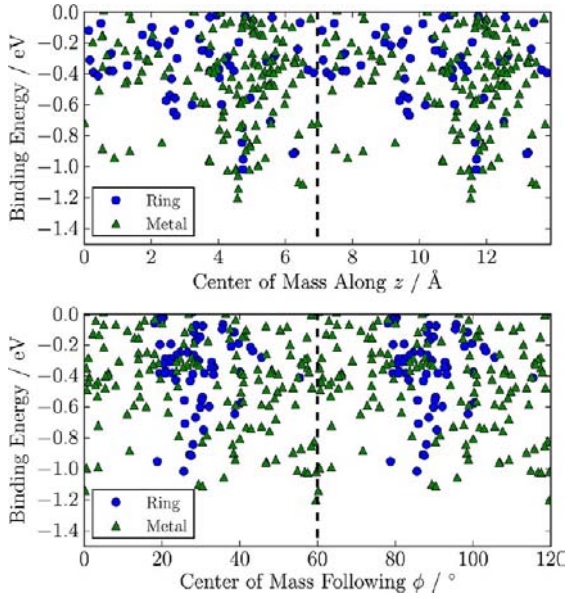

Figure 4. Au_8 CM distribution along the pore height, z, and azimuthal angle, ϕ, around the axis of the pore. The dashed lines indicate when the data is repeated due to periodic boundaries, making it easier to follow the data on the boundary between two unit cells.

406 distinct clusters that are distributed throughout the unit cell of the MOF. Every point on this figure represents a local minimum of the cluster's energy surface relaxed until the maximum force on any atom is below 0.05 eV/Å. The large number of distinct minima that exist is a clear illustration of the need to use a means of automated structure generation to explore these systems. Analogous plots showing the adsorption potential energy of the Pd_8 and Au_4Pd_4 clusters we examined are shown in Figures 5 and 6. These include 421 and 645 distinct clusters, respectively.

Figures 7−9 show the most stable candidate found from each run for each stoichiometry. The adsorption potential energy, local coordination, and DDEC charges for each structure are reported in Tables 2 and 3. Bond lengths are reported in Table S1 in the Supporting Information [SI]. The definition of when two atoms are coordinated was given in the previous section, and the adsorption energies are calculated using eq 1. To calculate E_b a reference structure for the isolated (i.e., gas phase) cluster is needed. For Au_8 the structure is taken from ref 56, for Pd_8, from ref 57, and for Au_4Pd_4 the GA was run to obtain the most stable structure. The isolated structures are shown in Figure 10 with more structures of Au_4Pd_4 shown in Figure S1 (SI). During the adsorption process the framework and cluster rearranges into a geometry optimizing the interaction between the MOF and cluster. If the cluster was not adsorbed in the framework, a deformation energy E_d would be associated with this rearrangement. By removing the cluster

dx.doi.org/10.1021/ja305004a | J. Am. Chem. Soc. 2012, 134, 12807−12816

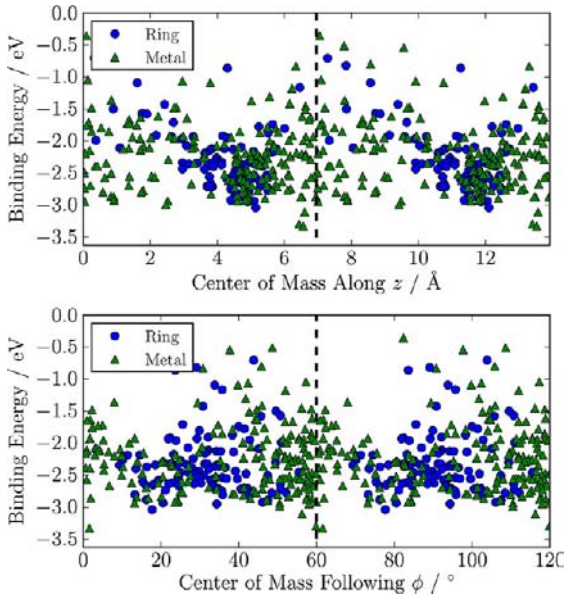

Figure 5. Pd_8 CM distribution along the pore height, z, and azimuthal angle, ϕ, around the axis of the pore.

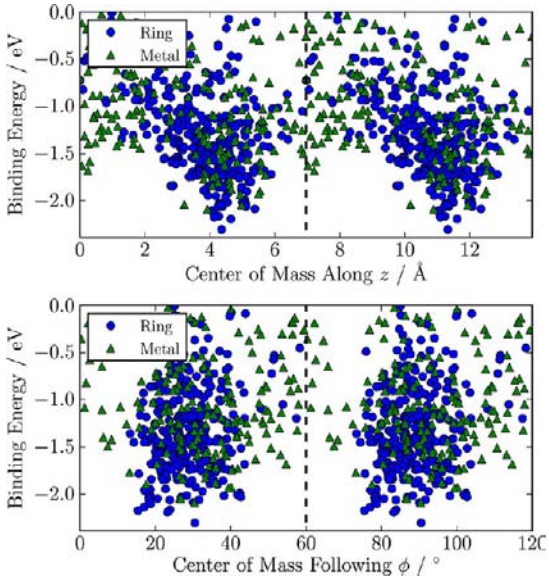

Figure 6. Au_4Pd_4 CM distribution both along the pore height, z, and azimuthal angle, ϕ, around the axis of the pore.

from the framework but keeping the geometry of the framework and cluster intact, this deformation energy can be calculated. The deformation energies $E_{d,MOF}$ and $E_{d,cluster}$ reported in Table 2 are calculated as the difference between the optimal geometry of either the MOF or the cluster compared to the geometry they are in when adsorbed. The total deformation energy during the adsorption processes is

$$E_{d,total} = E_{d,cluster} + E_{d,MOF}$$

The deformation energy is an energy paid to optimize the interaction between the cluster and the framework, and the total interaction energy between the two is thus the difference between the adsorption energy and the deformation energy:

$$E_I = E_b - E_{d,total} \quad (2)$$

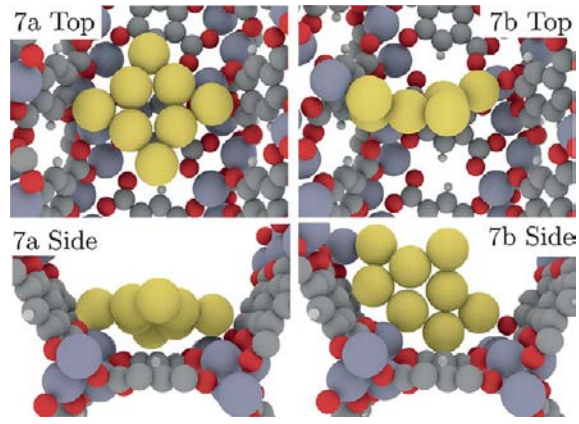

Figure 7. Top and side view of the most stable Au_8 candidate found in (a) the ring-centered run and (b) metal-centered run of the GA.

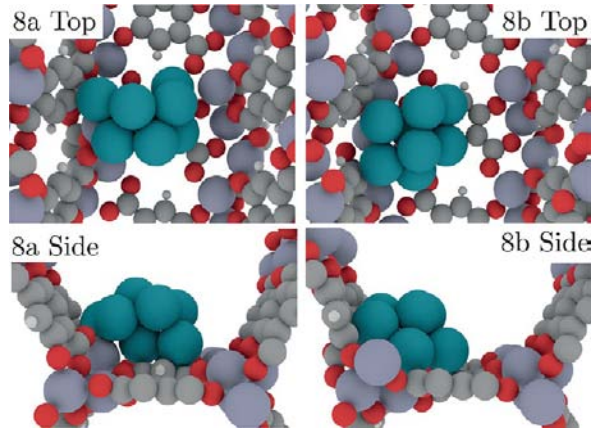

Figure 8. Top and side view of the most stable Pd_8 candidate found in (a) the ring-centered run and (b) metal-centered run of the GA.

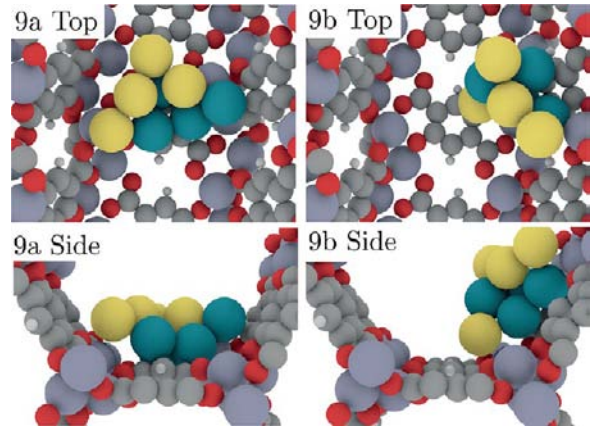

Figure 9. Top and side view of the most stable Au_4Pd_4 candidate found in (a) the ring-centered run and (b) metal-centered run of the GA.

For Au_8 the lowest energy structures from the two GA calculations are very different in their geometries and bond characteristics. The structure in Figure 7a has a planar structure closely resembling gas phase Au_8 (see Figure 10), whereas the structure in Figure 7b, in contrast, is strongly deformed and has more bonds to the framework. This observation is reflected in the deformation energies for each structure; the structure in Figure 7a has a deformation energy of only 0.05 eV whereas the

dx.doi.org/10.1021/ja305004a | J. Am. Chem. Soc. 2012, 134, 12807−12816

Table 2. Adsorption Energies and Deformation Energies for Structures Shown in Figures 7−9 Calculated Using Eqs 1−3[a]

	E_b	$E_{d,MOF}$	$E_{d,cluster}$	$E_{d,total}$	E_I
Au_8 - ring (Figure 7a)	−1.02	0.75	0.05	0.79	−1.81
Au_8 - metal (Figure 7b)	−1.20	2.60	0.71	3.31	−4.51
Pd_8 - ring (Figure 8a)	−3.04	1.81	0.40	2.21	−5.25
Pd_8 - metal (Figure 8b)	−3.32	3.43	0.61	4.04	−7.37
Au_4Pd_4 - ring (Figure 9a)	−2.30	3.00	1.42	4.42	−6.73
Au_4Pd_4 - metal (Figure 9b)	−2.09	1.26	1.04	2.30	−4.39

[a]All Energies in eV.

Table 3. Coordination and DDEC Charges for Each Structure Shown in Figures 7−9

	coordination (Au)	coordination (Pd)	charge (Au) (e)	charge (Pd) (e)
Au_8 - ring (Figure 7a)	2Zn, 1C, 1H	–	−0.22	–
Au_8 - metal (Figure 7b)	2Zn, 4C	–	−0.20	–
Pd_8 - ring (Figure 8a)	–	3Zn, 2O, 6C	–	−0.11
Pd_8 - metal (Figure 8b)	–	4Zn, 2O, 6C	–	−0.12
Au_4Pd_4 - ring (Figure 9a)	2Zn	2Zn, 6C	−0.33	0.24
Au_4Pd_4 - metal (Figure 9b)	2Zn	1Zn, 6C	−0.44	0.28

one in Figure 7b has a deformation energy of 0.71 eV. The same trend is seen in the surface deformation energies where the structure in Figure 7a has a surface deformation energy almost 4 times smaller than the one in Figure 7b. Although the structure in Figure 7a has the smallest deformation energy of the two, it is the one in Figure 7b that is the most stable cluster overall, with a binding energy 0.18 eV stronger than that of the structure in Figure 7a. When comparing the coordination of the two structures, it is seen that the one in Figure 7b coordinates to two atoms more than the structure in Figure 7a. It is surprising that two extra bonds can result in twice the interaction energy, but when comparing the bond lengths reported in Table S1 (SI) with the bond lengths for Au_1 it is seen that the structure in Figure 7b has Au−Zn and Au−C bond lengths much closer to the Au_1 ones.

For Pd_8 it is also the structure from the Zn-centered run of the GA which gives the most stable cluster. The cluster deformation energy is similar for the most stable cluster from the runs of the GA, but the framework deformation energy is almost 2 times larger for the structure in Figure 8b than for the one in Figure 8a. The framework deformation for the structure in Figure 8b is so large that one Zn atom is translated more than 1.6 Å from being an open metal site in the neighboring pore to coordinating directly to the Pd cluster. This explains why the structure in Figure 8b can be coordinated to four Zn atoms even though there are only three directly available and is a clear example of how framework flexibility plays an important role when strong covalent bonds are formed. The DDEC charges for Pd_8 show that this cluster gains charge from the framework, unlike the Pd monomer, which donated charge to the framework. This charge, however, is distributed across eight atoms so that the cluster can be considered almost neutral. Charge transfer is also small for Au_8. Comparing the bond strengths of Au_8 and Pd_8, it is seen that Pd_8 is bound almost 3 times more strongly to the framework than Au_8. This observation is consistent with the strongest Pd_1 bond being more than twice as strong as for Au_1. Table 3 shows that Pd_8 coordinates to 10 atoms in the framework, whereas Au_8 only coordinates with up to 5 atoms, emphasizing that Au has a lower affinity toward the framework than Pd.

We now consider the alloyed cluster Au_4Pd_4. The net binding energy observed for this cluster lies between Au_8 and Pd_8, as might be expected. One measure of the energy gained by alloying the two metals is

$$E_a = E(Au_4Pd_4) - \frac{E(Au_8) + E(Pd_8)}{2} \quad (3)$$

For the isolated clusters in Figure 10, $E_{a,vacuum}$ = −0.33 eV, showing that in the gas phase there is a considerable energy

Figure 10. Lowest energy vacuum structures of Au_8 (ref 56), Pd_8 (ref 57), and Au_4Pd_4, respectively.

gained by forming two Au_4Pd_4 clusters instead of having one Au_8 and one Pd_8 cluster. This is consistent with bulk calculations where 0.12 eV/atom is gained for the AuPd alloy compared to the pure metals.[58] For the supported clusters there is only a very weak bias toward alloying; for the most favored structure $E_{a,supported}$ = −0.04 eV.

The structures of the most stable Au_4Pd_4 clusters from each GA run are both centered on the aromatic ring, even though the structure in Figure 9b was produced from the metal-centered start population. This bias toward the ring is confirmed by looking at the azimuthal distribution in Figure 6, where both the metal-centered and ring-centered runs of the GA find structures primarily around 30°, corresponding to the top of the aromatic ring. This is in contrast to the nonalloyed clusters, where the most stable sites are on top of the Zn atoms and the azimuthal distributions in Figures 4 and 5 are close to being uniform across the cell. For both clusters, Pd atoms coordinate directly to the framework with Au atoms covering the Pd ones. This is consistent with the stronger binding of Pd to the framework and also consistent with Au having a 26% lower surface energy than Pd.[59,60] The charge transfer in the adsorbed clusters is dominated by charge exchange between the Au and Pd atoms with a magnitude similar to the isolated cluster, which has a charge transfer of −0.50e from the Pd to the Au atoms.

To gauge the accuracy of the PBE results we reexamined the structures from Figures 7−9 with the meta-GGA M06-L functional. The agreement between the two functionals should be good for Pd, but for Au larger changes might occur since the interaction between an aromatic ring and Au is underestimated with PBE.[46] The lattice parameters for MOF-74 with the M06-L functional are calculated and used for these calculations. The

shape of the unit cell is unchanged, but the volume of the cell is 9.1% larger than the experimental value, which is a larger deviation from the experimental result than with the PBE functional. The metal cluster binding energies have been calculated with the M06-L functional both in the PBE optimized and M06-L optimized cell. The cluster binding energies change less than 0.01 eV, showing a very weak dependence on lattice parameters.

The calculated adsorption energies and deformation energies for each functional are reported in Table 4 and the structures

Table 4. Comparison between PBE and M06-L Adsorption Potential Energies and Deformation Energies for the Clusters Shown in Figures 7−9[a]

	PBE		M06-L		
	$E_{b,PBE}$	$E_{d,PBE,total}$	$E_{b,M06-L}$	$E_{d,M06-L,total}$	$E_{b,PBE} - E_{d,M06-L}$
Au_8 - ring (Figure 7a)	−1.02	0.79	−2.61	0.59	1.59
Au_8 - metal (Figure 7b)	−1.20	3.31	−1.68	3.22	0.48
Pd_8 - ring (Figure 8a)	−3.04	2.21	−3.86	2.45	0.83
Pd_8 - metal (Figure 8b)	−3.32	4.04	−4.49	4.31	1.17
Au_4Pd_4 - ring (Figure 9a)	−2.30	4.42	−3.15	4.67	0.84
Au_4Pd_4 - metal (Figure 9b)	−2.09	2.30	−2.66	2.76	0.57

[a]All Energies in eV.

are shown in Figure S3 (SI). All structures are bound more strongly to the framework with the M06-L functional. For Pd_8 and Au_4Pd_4 the change is close to a constant shift of 1 and 0.7 eV, respectively. The energy gains are very different for the two Au_8 clusters we examined, however, leading to a change in which structure is the preferred. It is surprising that the structure in Figure 7b only gains 0.48 eV with the M06-L functional compared to the 1.59 eV that the structure in Figure 7a gains, since the deformation energy for both structures is reduced by a similar amount. This increase can be understood by an increased interaction between Au atoms and the aromatic ring. With the PBE functional the distance between the aromatic ring and the Au cluster is around 3.8 Å, whereas for the M06-L functional this distance decreases to around 3.3 Å. This finding is in agreement with previous studies of benzene adsorbed on Au(111) where it was shown that the PBE functional does not describe any significant binding but the M06-L functional gives a binding energy of 0.5 eV when the benzene ring is 3.2 Å from the Au surface.[46] Although these results point to some sensitivity in the relative energies of Au clusters to the DFT functional, performing calculations for the full range of clusters we explored in our GA calculations with M06-L or other functionals is beyond the scope of this article.

Mobility of Au_8 and Pd_8 in MOF-74. Understanding the equilibrium structure of adsorbed clusters of fixed size in MOF-74 gives only partial information about the form and size that adsorbed metals in this MOF can be expected to take. In most environments containing multiple metal clusters, there is a driving force for smaller clusters to agglomerate into larger clusters. One way that this can happen is by net diffusion of clusters. In this section, we introduce methods that give some insight into the diffusional mobility of Au and Pd clusters along the pores of MOF-74. The methods developed here are transferable to the alloyed clusters, but an investigation of alloy diffusion is outside the scope of this contribution.

There are a variety of examples where a linear relationship exists between the adsorption enthalpy and the transition state energy for a given reaction.[61,62] This relation is known as the Brønsted−Evans−Polanyi (BEP) relation,[63,64] and it hints that the diffusion barrier for Pd_8 will be higher than for Au_8 since Pd_8 is bound about 3 times stronger to the framework. Having established the optimal structure of Au_8 and Pd_8 in MOF-74 we are in a position to calculate a lower bound on the diffusion rate of these clusters in the framework. The large number of candidates found distributed through the MOF unit cell makes it possible to find a good initial guess for a diffusion path from one unit cell to the next through the identified structures. Nudged elastic band (NEB) calculations[65] together with the climbing image NEB method[66] (CI-NEB) can then be used to interpolate and refine this initial guess until a full path including one or several transition states is found.

Since the number of Au_8 and Pd_8 adsorption geometries found is 406 and 421, respectively, an algorithm is needed that can give the shortest path through these structures from an initial structure to that same structure translated one unit cell along the z direction. To calculate the distance between two structures a distance measure must be defined. For two configurations i and j the distance between the two clusters is defined as

$$d_{ij} = \min_m \sqrt{\sum_{k=1}^{8} (\bar{r}_i(k) - \bar{r}_j(f_m(k))^2}$$

with f_m returning the mth permutation of the integers 1−8. Changes in the framework structure are ignored in this expression since the sum is only over the cluster indices. For each pair i and j there are 8! = 40320 distances that need to be compared, and for N configurations there are $N^2 \cdot 8!/2$ in total, with the factor of 2 coming from $d_{ij} = d_{ji}$. When a table of all $N^2/2$ shortest distances has been calculated, Dijkstra's algorithm[67] can be used to calculate the shortest path from a given start candidate to all other candidates. If d_{ij} is used as the distance between two candidates, the shortest path from the start to end configuration will be the direct path without any intermediate states. Since we want to identify intermediate states to pass through, we instead use d_{ij}^2 as a distance measure since it will increase the cost of long distances, thus making the shortest path pass through intermediate configurations. To further improve on the path, a requirement on the energy can be imposed. For Au_8 (Pd_8) we chose to only consider structures that lie within 0.50 (1.0) eV from the starting candidate.

We first consider this process for the diffusion of Au_8. We limit the investigation to the structure in Figure 7a since it is the most stable structure with the M06-L functional. A full NEB path is shown in Figure 11, with the two unique structures proposed by the shortest path algorithm marked with an S. Local minima along the path are indicated with red triangles, and NEB calculations have been performed between each of them. Square (circular) markers indicate segments computed with CI-NEB (NEB) forces. CI-NEB calculations are done on all segments containing significant maxima. The motion of Au_8 starts by detaching the topmost Au in Figure 11a from the aromatic ring. After this atom is free, the Au cluster moves forward by alternate rotations around the right and left Au

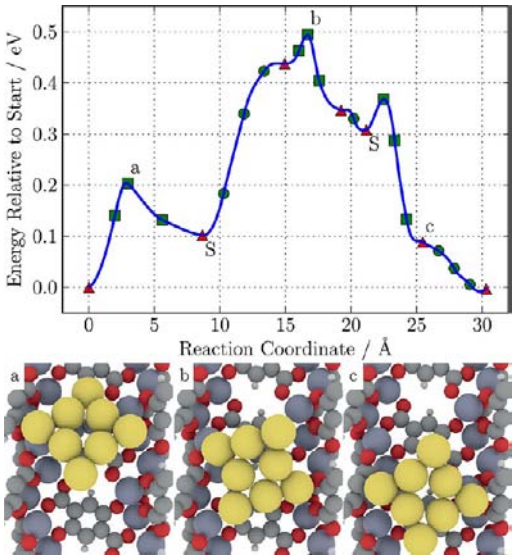

Figure 11. NEB path for the diffusion of Au_8 in the framework. The start and end points consist of the structure in Figure 7a, and structures marked with an S were found using the shortest path algorithm. Squares (circles) indicate points along a CI-NEB (NEB) path. Triangles indicate stable local minima.

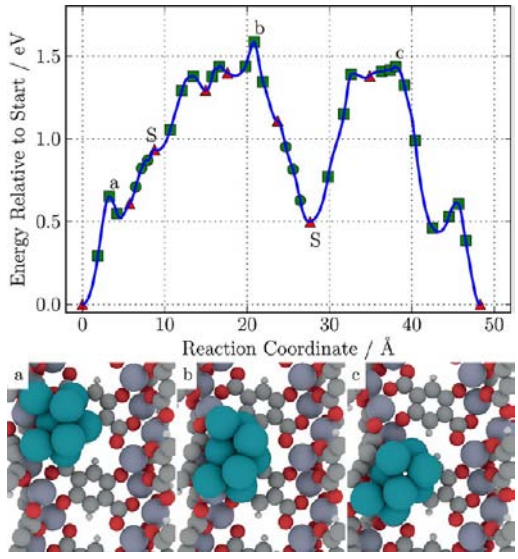

Figure 12. NEB path for the diffusion of Pd_8 in the framework. The start and end points consist of the structure in Figure 8b, and structures marked with an S were found using the shortest path algorithm. Squares (circles) indicate points along a CI-NEB (NEB) path. Triangles indicate stable local minima.

atom shown in Figure 11a–c. The transition state energy $E_{T,Au}$ is the highest energy along the diffusion path relative to the starting structure, which for the path we have considered is 0.49 eV. The transition state energy is similar to the binding energy of Au_1, which is not surprising since the diffusion proceeds by breaking one Au–substrate bond at a time. It is important to remember that this diffusion barrier is only an upper bound and it is possible that transitions with lower activation energies exist. With a transition state energy less than 0.5 eV it is clear that Au_8 clusters will be mobile in MOF-74 even at low temperatures because of the low energy barrier for net diffusion of these clusters.

Now considering Pd_8, the shortest path method can again be used to find a good initial guess along the path. We chose here only to investigate the structure in Figure 8b, since it is the structure bound most strongly to the framework. Figure 12 shows the resulting diffusion path together with three characteristic configurations. The initial path again contains two unique structures with an additional six local minima found along the path. The net diffusion barrier is in this case $E_{T,Pd}$ = 1.59 eV. The diffusion of Pd_8 follows a considerably different path than Au_8. For Au_8 the overall shape of the cluster is unchanged along the path, whereas the Pd_8 cluster remains compact and deforms considerably as it moves along the MOF by what can be described as a rolling motion. Although, as above, this calculation provides only an upper bound on the diffusion activation energy of the cluster, our results suggest that Pd clusters are considerably less mobile in MOF-74 than Au clusters.

Comparing the diffusion barrier for Au_8 and Pd_8 we see that the ratio between the adsorption potential energy E_b and the diffusion barrier E_T is ~2.1 for both species, hinting that the mobility of adsorbed particles can be predicted from their adsorption energies. This is a result that to our knowledge has not been observed before for the diffusion of nanosized Au and Pd particles using ab initio methods. From the diffusion barriers it is now possible to calculate the rate of diffusion by assuming an Arrhenius equation for the diffusion rate and assuming an attempt rate of 1.0×10^{14} s^{-1}. At room temperature Au_8 will jump more than half a million times per second, whereas the diffusion of Pd_8 will happen 18 orders of magnitude slower, i.e. once every 10^{12} s. It is thus likely that Pd_8 will remain dispersed throughout the framework whereas Au_8 particles will not. The successful use of MOFs as an Au support framework will thus require either a stronger interaction between the MOF and the Au cluster, by functionalizing the Au or by changing the MOF, or the framework needs some geometrical feature, such as narrow windows, to limit the diffusion. One experimental example combining both effects is the adsorption of Au in ZIF-90. The narrow windows (3.5 Å) of ZIF-90 combined with the aldehyde groups in the framework are enough to localize Au particles in a size matching the size of the cavities.[25] Another example is the adsorption of functionalized Au_2 and Au_3 particles in a MOF containing fluorinated channels. The combination of functionalizing the Au before adsorption together with the very reactive hydrophobic channels of the MOF is enough to stabilize the small clusters under atmospheric conditions for up to six months.[68]

Framework Alterations. The correlation between the diffusion barrier and adsorption energy of adsorbed clusters suggests that the energy barrier for diffusion can be increased if the cluster's adsorption energy is increased. This would be desirable in an effort to develop systems in which adsorbed metal clusters were stable (or perhaps metastable) against agglomeration. One way to increase the adsorption energy would be by altering the MOF-74 framework to make it more reactive. MOF-74 is one of a set of isostructural MOFs where the Zn atoms can be substituted by Mg, Mn, Co, or Ni.[31] For H_2 adsorption a 35% increase in binding energy is observed using Mg instead of Zn in the MOF.[31] Since the metal clusters coordinate primarily to C atoms the effect of a metal substitution is expected to be less in this case, although charge rearrangements or other electronic effects might affect the result. The binding energies of the structures from Figures 4 and 5 with Zn substituted with Mg are shown in Table 5. These calculations are done using the DFT optimized unit cell of Mg-

dx.doi.org/10.1021/ja305004a | J. Am. Chem. Soc. 2012, 134, 12807–12816

Table 5. Adsorption Potential Energies for Structures Shown in Figures 7−9 with Alterations Done to the Framework[a]

	Mg-MOF-74		pyridine	
	E_b	$E_{d,total}$	E_b	$E_{d,total}$
Au_8 - ring (Figure 7a)	−1.03	0.52	−1.53	0.93
Au_8 - metal (Figure 7b)	−0.48	3.07	−1.04	3.08
Pd_8 - ring (Figure 8a)	−2.88	1.60	−2.58	2.11
Pd_8 - metal (Figure 8b)	−2.07	4.47	−3.36	3.03
Au_4Pd_4 - ring (Figure 9a)	−1.95	2.51	−2.02	4.47
Au_4Pd_4 - metal (Figure 9b)	−1.88	1.98	−1.82	2.43

[a]All Energies in eV.

MOF-74, which has a volume 1.1% larger than MOF-74; a change which is in good agreement with experiments.[31] From Table 5 it is seen that all candidates are bound more weakly to the Mg-MOF-74 framework than to MOF-74, except the structure in Figure 7a that is unchanged. The adsorbed geometries are shown in Figure S4 (SI). It may be possible that the full GA approach would identify configurations that bind clusters more strongly in Mg-MOF-74, but the limited evidence from our results suggests that using the Mg material will not significantly enhance cluster binding energies.

Another plausible, although not experimentally tested, substitution is to replace the aromatic ring with a pyridine molecule, since an N atom is expected to have a stronger interaction with surrounding atoms than a CH group. The orientation of the pyridine molecule is chosen such that the N atom is close to the adsorbed cluster (see Figure S5 [SI]). The adsorption energies for these substitutions are also reported in Table 5. The calculations are done using the DFT optimized unit cell of N-MOF-74, which is changed by 1.1% compared to MOF-74. These calculations assume that the N-substituted MOF is isostructural to MOF-74; we know of no experimental evidence to test this assumption. In this case the structure in Figure 7a has its binding energy increased dramatically, which is not surprising since the top Au atom in Figure 7a is now coordinated directly to a N atom instead of a CH group. All other clusters, however, bind similarly or more weakly to the framework than in MOF-74. This initial set of calculations for pyridine-substituted MOF-74 hints that framework substitutions of this kind may be an avenue to enhancing the binding energy of adsorbed metal clusters in MOFs, but conclusive results require rerunning the GA.

SUMMARY

The adsorption of Au, Pd, and AuPd in MOF-74 has been investigated with a genetic algorithm (GA) employing DFT calculations for local relaxations. This is the first time that the structure of metal clusters adsorbed in a MOF has been studied theoretically. From the investigation of Au_8, Pd_8, and Au_4Pd_4 it can be concluded that Au is bound roughly 3 times more weakly to the framework than Pd and that at this cluster size no significant energy is gained by alloying the two metals. Although MOF-74 includes open metal sites, our results indicate that these sites do not play a special role compared to the rest of the framework in the stabilization of metal clusters.

A key aspect of our results is that our method generates large numbers of distinct cluster structures. The results from these calculations give a degree of confidence in predicting the structure of these complex clusters that could not be achieved by examining a small number of candidate clusters "by hand". From the large set of clusters found for Au_8 and Pd_8, a method was developed for calculating an upper bound on the diffusion barrier for these adsorbed metal clusters. It was shown that a linear relationship exists between the adsorption energy and the diffusion barrier, which shows that, if one wants to decrease the mobility of supported Au clusters, one needs to increase their binding energy. Two alterations to the framework were tested, but no systematic increase in binding energies was observed.

An alternative approach to making small metal clusters that are stable against agglomeration is to consider other MOF frameworks as potential hosts for adsorbed clusters. Two complementary avenues could be explored. The first one relies on increasing the binding energy of the adsorbed cluster. In the case of Au this does not seem likely without making a very reactive framework, which for catalytic applications might produce other difficulties. A second avenue is instead to rely on geometrical features of the MOF. Although MOFs with a wide variety of pore topologies exist, a particularly interesting situation is MOFs consisting of a combination of cavities with a diameter of 1−2 nm separated by narrow windows of 0.5 nm or less. The diffusion of clusters larger than 0.5 nm through these windows will therefore be associated with a large barrier due to steric hindrance. The ideal MOF for cluster adsorption would have a topology such that there is an energetically optimal cluster size due to the limiting confines of the framework, while still keeping the clusters accessible for catalytic reactions.

ASSOCIATED CONTENT

Supporting Information

Figure of four additional structures of Au_4Pd_4 in vacuum, detailed information about the MOF-particle coordination for Au_8-, Pd_8-, and Au_4Pd_4 and figures of the adsorbed clusters as calculated with the M06-L functional and after Mg and N substitutions. This material is available free of charge via the Internet at http://pubs.acs.org.

AUTHOR INFORMATION

Corresponding Author

david.sholl@chbe.gatech.edu

Notes

The authors declare no competing financial interest.

ACKNOWLEDGMENTS

D.S.S. received partial support from the National Science Foundation (Grant 0966582) and the Center for Atomic Level Catalyst Design, an Energy Frontier Research Center funded by the U.S. Department of Energy, Office of Science, Office of Basic Energy Sciences under DE-SC0001058 (Center for Atomic Level Catalyst Design). K.S.W. received partial support from the National Science Foundation (CAREER Award 969261) and the Army Research Office Contract W911NF-10-0079. L.B.V. received support from the Lundbeck Foundation. All calculations were carried out with support from the Danish Center for Scientific Computing (DCSC). We thank Bjørk Hammer for many helpful discussions.

REFERENCES

(1) Li, H.; Eddaoudi, M.; O'Keeffe, M.; Yaghi, O. M. *Nature* **1999**, *402*, 276.
(2) Ferey, G. *Chem. Soc. Rev.* **2008**, *37*, 191.
(3) Yaghi, O.; O'Keeffe, M.; Ockwig, N.; Chae, H.; Eddaoudi, M.; Kim, J. *Nature* **2003**, *423*, 705.
(4) Wilmer, C.; Leaf, M.; Lee, C.; Farha, O.; Hauser, B.; Hupp, J.; Snurr, R. *Nature Chem.* **2012**, *4*, 83.
(5) Haldoupis, E.; Nair, S.; Sholl, D. *J. Am. Chem. Soc.* **2010**, *132*, 7528.
(6) Haldoupis, E.; Nair, S.; Sholl, D. *J. Am. Chem. Soc.* **2012**, *134*, 4313.
(7) Li, J.-R.; Kuppler, R.; Zhou, H.-C. *Chem. Soc. Rev.* **2009**, *38*, 1477.
(8) Keskin, S.; van Heest, T. M.; Sholl, D. S. *ChemSusChem* **2010**, *3*, 879.
(9) Liu, Y.; Kabbour, H.; Brown, C.; Neumann, D.; Ahn, C. *Langmuir* **2008**, *24*, 4772.
(10) Murray, L.; Dinca, M.; Long, J. *Chem. Soc. Rev.* **2009**, *38*, 1294.
(11) Horcajada, P.; Chalati, T.; Serre, C.; Gillet, B.; Sebrie, C.; Baati, T.; Eubank, J.; Heurtaux, D.; Clayette, P.; Kreuz, C.; Chang, J.-S.; Hwang, Y.; Marsaud, V.; Bories, P.-N.; Cynober, L.; Gil, S.; Ferey, G.; Couvreur, P.; Gref, R. *Nat. Mater.* **2010**, *9*, 172.
(12) Allendorf, M. D.; Bauer, C. A.; Bhakta, R. K.; Houk, R. J. T. *Chem. Soc. Rev.* **2009**, *38*, 1330.
(13) Lee, J.; Farha, O.; Roberts, J.; Scheidt, K.; Nguyen, S.; Hupp, J. *Chem. Soc. Rev.* **2009**, *38*, 1450.
(14) Ma, L.; Abney, C.; Lin, W. *Chem. Soc. Rev.* **2009**, *38*, 1248.
(15) Seo, J.; Whang, D.; Lee, H.; Jun, S.; Oh, J.; Jeon, Y.; Kim, K. *Nature* **2000**, *404*, 982.
(16) Gu, X.; Lu, Z.-H.; Jiang, H.-L.; Akita, T.; Xu, Q. *J. Am. Chem. Soc.* **2011**, *133*, 11822.
(17) Jiang, H.-L.; Liu, B.; Akita, T.; Haruta, M.; Sakurai, H.; Xu, Q. *J. Am. Chem. Soc.* **2009**, *131*, 11302.
(18) Müller, M.; Turner, S.; Lebedev, O.; Wang, Y.; van Tendeloo, G.; Fischer, R. *Eur. J. Inorg. Chem.* **2011**, *2011*, 1876.
(19) Hashmi, A. S. K.; Hutchings, G. J. *Angew. Chem., Int. Ed.* **2006**, *45*, 7896.
(20) Hermes, S.; Schröter, M.-K.; Schmid, R.; Khodeir, L.; Muhler, M.; Tissler, A.; Fischer, R.; Fischer, R. *Angew. Chem., Int. Ed.* **2005**, *44*, 6237.
(21) Liu, H.; Liu, Y.; Li, Y.; Tang, Z.; Jiang, H. *J. Phys. Chem. C* **2010**, *114*, 13362.
(22) Huang, Y.; Lin, Z.; Cao, R. *Chem.—Eur. J.* **2011**, *17*, 12706.
(23) Pan, Y.; Yuan, B.; Li, Y.; He, D. *Chem. Commun.* **2010**, *46*, 2280.
(24) Jiang, H.-L.; Akita, T.; Ishida, T.; Haruta, M.; Xu, Q. *J. Am. Chem. Soc.* **2011**, *133*, 1304.
(25) Esken, D.; Turner, S.; Lebedev, O.; Van Tendeloo, G.; Fischer, R. *Chem. Mater.* **2010**, *22*, 6393.
(26) Lu, G.; Li, S.; Guo, Z.; Farha, O.; Hauser, B.; Qi, X.; Wang, Y.; Wang, X.; Han, S.; Liu, X.; DuChene, J.; Zhang, H.; Zhang, Q.; Chen, X.; Ma, J.; Loo, S.; Wei, W.; Yang, Y.; Hupp, J.; Huo, F. *Nature Chem.* **2012**, *4*, 310.
(27) Schröder, F.; Esken, D.; Cokoja, M.; van den Berg, M.; Lebedev, O.; Van Tendeloo, G.; Walaszek, B.; Buntkowsky, G.; Limbach, H.-H.; Chaudret, B.; Fischer, R. *J. Am. Chem. Soc.* **2008**, *130*, 6119.
(28) Meilikhov, M.; Yusenko, K.; Esken, D.; Turner, S.; Van Tendeloo, G.; Fischer, R. *Eur. J. Inorg. Chem.* **2010**, *2010*, 3701.
(29) Keskin, S.; Liu, J.; Rankin, R.; Johnson, K.; Sholl, D. *Ind. Eng. Chem. Res.* **2008**, *48*, 2355.
(30) Getman, R.; Bae, Y.-S.; Wilmer, C.; Snurr, R. *Chem. Rev.* **2012**, *112*, 703.
(31) Zhou, W.; Wu, H.; Yildirim, T. *J. Am. Chem. Soc.* **2008**, *130*, 15268.
(32) Choi, S.; Watanabe, T.; Bae, T.-H.; Sholl, D.; Jones, C. *J. Phys. Chem. Lett.* **2012**, 1136.
(33) Cuenya, B. *Thin Solid Films* **2010**, *518*, 3127.
(34) Baletto, F.; Ferrando, R. *Rev. Mod. Phys.* **2005**, *77*, 371.
(35) Vilhelmsen, L.; Hammer, B. *Phys. Rev. Lett.* **2012**, *108*, 126101.
(36) Chen, M.; Kumar, D.; Yi, C.-W.; Goodman, W. *Science* **2005**, *310*, 291.
(37) Zhou, X.; Huang, Y.; Xing, W.; Liu, C.; Liao, J.; Lu, T. *Chem. Commun.* **2008**, 3540.
(38) Rosi, N.; Kim, J.; Eddaoudi, M.; Chen, B.; O'Keeffe, M.; Yaghi, O. *J. Am. Chem. Soc.* **2005**, *127*, 1504.
(39) Enkovaara, J.; Rostgaard, C.; Mortensen, J. J.; Chen, J.; Dułak, M.; Ferrighi, L.; Gavnholt, J.; Glinsvad, C.; Haikola, V.; Hansen, H. A.; Kristoffersen, H. H.; Kuisma, M.; Larsen, A. H.; Lehtovaara, L.; Ljungberg, M.; Lopez-Acevedo, O.; Moses, P. G.; Ojanen, J.; Olsen, T.; Petzold, V.; Romero, N. A.; Stausholm-Møller, J.; Strange, M.; Tritsaris, G. A.; Vanin, M.; Walter, M.; Hammer, B.; Häkkinen, H.; Madsen, G. K. H.; Nieminen, R. M.; Nørskov, J. K.; Puska, M.; Rantala, T. T.; Schiøtz, J.; Thygesen, K. S.; Jacobsen, K. W. *J. Phys.: Condens. Matter* **2010**, *22*, 253202.
(40) Mortensen, J. J.; Hansen, L. B.; Jacobsen, K. W. *Phys. Rev. B* **2005**, *71*, 035109.
(41) Blöchl, P. E. *Phys. Rev. B* **1994**, *50*, 17953.
(42) Larsen, A. H.; Vanin, M.; Mortensen, J. J.; Thygesen, K. S.; Jacobsen, K. W. *Phys. Rev. B* **2009**, *80*, 195112.
(43) Perdew, J.; Burke, K.; Ernzerhof, M. *Phys. Rev. Lett.* **1996**, *77*, 3865.
(44) Ferrighi, L.; Hammer, B.; Madsen, G. *J. Am. Chem. Soc.* **2009**, *131*, 10605.
(45) Zhao, Y.; Truhlar, D. *J. Chem. Phys.* **2006**, *125*, 194101.
(46) Ferrighi, L.; Madsen, G.; Hammer, B. *J. Chem. Phys.* **2011**, *135*, 084704.
(47) Shamov, G.; Budzelaar, P.; Schreckenbach, G. *J. Chem. Theory Comput.* **2010**, *6*, 477.
(48) Leverentz, H.; Truhlar, D. *J. Phys. Chem. A* **2008**, *112*, 6009.
(49) Deaven, D. M.; Ho, K. M. *Phys. Rev. Lett.* **1995**, *75*, 288.
(50) Wales, D.; Scheraga, H. *Science* **1999**, *285*, 1368.
(51) Sykes; Williams, F.; Tikhov, M.; Lambert, R. *J. Phys. Chem. B* **2002**, *106*, 5390.
(52) Johnston, R. *Dalton Trans.* **2003**, *22*, 4193.
(53) Manz, T.; Sholl, D. *J. Chem. Theory Comput.* **2010**, *6*, 2455.
(54) Manz, T.; Sholl, D. *J. Chem. Theory Comput.* **2011**, *7*, 4146.
(55) Martinez, U.; Vilhelmsen, L.; Kristoffersen, H.; Møller, J.; Hammer, B. *Phys. Rev. B* **2011**, *84*, 205434.
(56) Assadollahzadeh, B.; Schwerdtfeger, P. *J. Chem. Phys.* **2009**, *131*, 064306.
(57) Zanti, G.; Peeters, D. *Eur. J. Inorg. Chem.* **2009**, *2009*, 3904.
(58) Sluiter, M.; Colinet, C.; Pasturel, A. *Phys. Rev. B* **2006**, *73*, 174204.
(59) Mezey, L. Z.; Giber, J. *Jpn. J. Appl. Phys.* **1982**, *21*, 1569.
(60) Tyson, W. R.; Miller, W. A. *Surf. Sci.* **1977**, *62*, 267.
(61) Logadottir, A. *J. Catal.* **2001**, *197*, 229.
(62) Bligaard, T.; Nørskov, J. K.; Dahl, S.; Matthiesen, J.; Christensen, C. H.; Sehested, J. *J. Catal.* **2004**, *224*, 206.
(63) Evans, M. G.; Polanyi, M. *Trans. Faraday Soc.* **1938**, *34*, 11.
(64) Bronsted, J. N. *Chem. Rev.* **1928**, *5*, 231.
(65) Henkelman, G.; Jónsson, H. *J. Chem. Phys.* **2000**, *113*, 9978.
(66) Henkelman, G.; Uberuaga, B.; Jónsson, H. *J. Chem. Phys.* **2000**, *113*, 9901.
(67) Dijkstra, E. W. *Numerische Mathematik* **1959**, *1*, 269.
(68) Jiang, H.-L.; Lin, Q.-P.; Akita, T.; Liu, B.; Ohashi, H.; Oji, H.; Honma, T.; Takei, T.; Haruta, M.; Xu, Q. *Chem.—Eur. J.* **2011**, *17*, 78.